CHAPTER THREE

Experimental Technique

3.1 Introduction

In the following sections we demonstrate the sample preparation and characterization methods in this work. Chitosan (CS) is employed as a host polymer in the present study to prepare solid polymer electrolytes (SPEs) and nanocomposite solid polymer electrolytes (NCSPEs). Three different SPE films were prepared i.e. $CS-AgCF_3SO_3$, $CS-NaCF_3SO_3$, and $CS-LiCF_3SO_3$. To prepare NCPE films nano-Al_2O_3 (size <50 nm) filler was added in different concentrations to the highest amorphous sample of each SPE system. The structure and morphology of all the SPEs and NCPEs were characterized using X-ray diffractogram (XRD), scanning electron microscopy (SEM), and energy dispersive analysis of X-rays (EDX). Ultraviolet-visible (UV-Vis) absorption spectroscopy and transmission electron microscopy (TEM) were also used to investigate the formation of silver nanoparticles in $CS-AgCF_3SO_3$ system. Finally, electrochemical impedance spectroscopy (EIS) was carried out on all SPEs and NCPEs to study the electrical and dielectric property.

3.2 Experimental Details

3.2.1 Raw Materials

Chitosan from crab shells ($\geq$75% deacetylated, Sigma Aldrich), silver triflate ($AgCF_3SO_3$), sodium triflate ($NaCF_3SO_3$), lithium triflate ($LiCF_3SO_3$) and aluminum oxide (Al_2O_3, size < 50 nm) were supplied by sigma Aldrich. Acetic acid (1%) was prepared using glacial acetic acid solution and used as the solvent in casting solid and nano-composite polymer electrolytes.

3.2.2 Preparation of Chitosan:XCF_3SO_3 (X=Ag, Na and Li) SPE thin films

The SPE films were prepared by the solution cast technique. For this purpose 1 gm of chitosan was dissolved in 100 ml of 1 % acetic acid solution. The mixture was stirred continuously with a magnetic stirrer for several hours at room temperature until the chitosan powder has completely dissolved in the acetic acid solution. To these sets of solutions 2 wt. % to 10 wt. % silver triflate were added separately and the mixtures were stirred continuously until homogeneous solutions were obtained. The solutions were then cast into different clean and dry petri dish and allowed to evaporate at room temperature until solvent-free films were obtained. The films were kept in desiccators with blue silica gel desiccant for further drying. Table 3.1 shows the concentration of the prepared samples. Chitosan:$NaCF_3SO_3$ and chitosan:$LiCF_3SO_3$ solid polymer electrolytes were also prepared following the same procedure as described for Chitosan:$AgCF_3SO_3$. Table 3.1 shows the concentration of the chitosan:$AgCF_3SO_3$ solid polymer electrolyte samples.

Table 3.1 composition of chitosan:AgCF$_3$SO$_3$ SPE samples

Designation	Chitosan(g)	AgCF$_3$SO$_3$ (g)	AgCF$_3$SO$_3$ (wt. %)
CSA1	1.0	0.0000	0.0
CSA2	1.0	0.0204	2.0
CSA3	1.0	0.0416	4.0
CSA4	1.0	0.0638	6.0
CSA5	1.0	0.0869	8.0
CSA6	1.0	0.1111	10

CSA1 to CSA6 represent the code of SPE compositions based on CS:AgTf. Table 3.2 represents the composition of solid polymer electrolytes based on Chitosan:NaCF$_3$SO$_3$.

Table 3.2 composition of chitosan:NaCF$_3$SO$_3$ SPE samples

Designation	Chitosan(g)	NaCF$_3$SO$_3$ (g)	NaCF$_3$SO$_3$ (wt. %)
CSB1	1.0	0.0000	0.0
CSB2	1.0	0.0204	2.0
CSB3	1.0	0.0416	4.0
CSB4	1.0	0.0638	6.0
CSB5	1.0	0.0869	8.0
CSB6	1.0	0.1111	10

CSB1 to CSB6 represent the code of SPE compositions based on CS:NaTf. Table 3.3 represents the composition of solid polymer electrolyte based on Chitosan:LiCF$_3$SO$_3$.

Table 3.3 composition of chitosan:LiCF$_3$SO$_3$ SPE samples

Designation	Chitosan(g)	LiCF$_3$SO$_3$ (g)	LiCF$_3$SO$_3$ (wt. %)
CSC1	1.0	0.0000	0.0
CSC2	1.0	0.0204	2.0
CSC3	1.0	0.0416	4.0
CSC4	1.0	0.0638	6.0
CSC5	1.0	0.0869	8.0
CSC6	1.0	0.1111	10

CSC1 to CSC6 represent the code of SPE compositions based on CS:LiTf.

3.2.3 Preparation of NCPE films using Al$_2$O$_3$ as a nano size (size < 50 nm) filler

The highest conducting sample in each of the three systems was selected to prepare NCPEs as follows. Initially the chitosan and silver triflate (90:10) were dissolved in acetic acid to obtain homogeneous solutions as described in section 3.2.2. To prepare NCPEs, the Al$_2$O$_3$ were first dispersed in 20 ml acetic acid solution and stirred. The Al$_2$O$_3$ concentrations were varied from 2 % to 10 %. The Al$_2$O$_3$ dispersoids were mixed with chitosan:silver triflate (90:10) solutions and then continuously stirred. The solutions were then cast into different clean and dry petri dish and allowed to evaporate at room temperature until solvent-free NCPE films were obtained. The films were kept in desiccators with blue silica gel desiccant for further drying. Table 3.4 shows the concentration of the prepared $(1-x)(0.9CS:0.1AgTf)-xAl_2O_3 (0.02 \leq x \leq 0.1)$ NCPEs. The other NCPE systems, such as $(1-x)(0.9CS:0.1NaTf)-xAl_2O_3 (0.02 \leq x \leq 0.1)$ and (1-

x)(0.9CS:0.1LiTf)-xAl$_2$O$_3$(0.02 $\leq$ x $\leq$ 0.1) were prepared by the same procedure as

described for (1-x) (0.9 Chitosan:0.1AgTf)-x Al$_2$O$_3$ (0.02 $\leq$ 0.1) previously.

Table 3.4 composition of (1-x)(0.9CS:0.1AgTf)-xAl$_2$O$_3$ (0.02 $\leq$ x $\leq$ 0.1) NCPEs

Designation	CS:AgTf = 90:10 (g)	Al$_2$O$_3$ (g)	Al$_2$O$_3$ (wt. %)
CSNA1	1.1111	0.0227	2.0
CSNA2	1.1111	0.0463	4.0
CSNA3	1.1111	0.0709	6.0
CSNA4	1.1111	0.0966	8.0
CSNA5	1.1111	0.1235	10

CSNA1 to CSNA6 represent the sample code of NCPE compositions of (1-

x)(0.9CS:0.1AgTf)-xAl$_2$O$_3$ (0.02 $\leq$ x $\leq$ 0.1). Table 3.5 represents the composition of (1-

x)(0.9CS:0.1NaTf)-xAl$_2$O$_3$ (0.02 $\leq$ x $\leq$ 0.1) NCPE.

Table 3.5 composition of (1-x)(0.9CS:0.1NaTf)-xAl$_2$O$_3$ (0.02 $\leq$ x $\leq$ 0.1) NCPEs

Designation	CS:NaTf = 90:10 (g)	Al$_2$O$_3$ (g)	Al$_2$O$_3$ (wt. %)
CSNB1	1.1111	0.0227	2.0
CSNB2	1.1111	0.0463	4.0
CSNB3	1.1111	0.0709	6.0
CSNB4	1.1111	0.0966	8.0
CSNB5	1.1111	0.1235	10

CSNB1 to CSNB6 represent the sample code of NCPE compositions of $(1-x)(0.9CS:0.1NaTf)-xAl_2O_3$ $(0.02 \leq x \leq 0.1)$. Table 3.6 Represents the composition of $(1-x)(0.9CS:0.1LiTf)-xAl_2O_3$ $(0.02 \leq x \leq 0.1)$ NCPEs.

.

Table 3.6 composition of $(1-x)(0.9CS:0.1LiTf)-xAl_2O_3$ $(0.02 \leq x \leq 0.1)$ NCPEs

Designation	CS:LiTf = 90:10 (g)	Al_2O_3 (g)	Al_2O_3 (wt. %)
CSNC1	1.1111	0.0227	2.0
CSNC2	1.1111	0.0463	4.0
CSNC3	1.1111	0.0709	6.0
CSNC4	1.1111	0.0966	8.0
CSNC5	1.1111	0.1235	10

CSNC1 to CSNC6 represent the sample code of $(1-x)(0.9CS:0.1LiTf)-xAl_2O_3$ $(0.02 \leq x \leq 0.1)$ NCPE compositions.

3.3 Electrical Measurements

The complex impedance spectroscopy was used to characterize the electrical properties of the materials. The sample films were cut into small discs of 2 cm diameter and sandwiched between two stainless steel (SS) blocking electrodes under spring pressure as depicted in Fig. 3.1. A digital micrometer (Mitutoyo Corp.) was used to measure the thickness of the sample films.
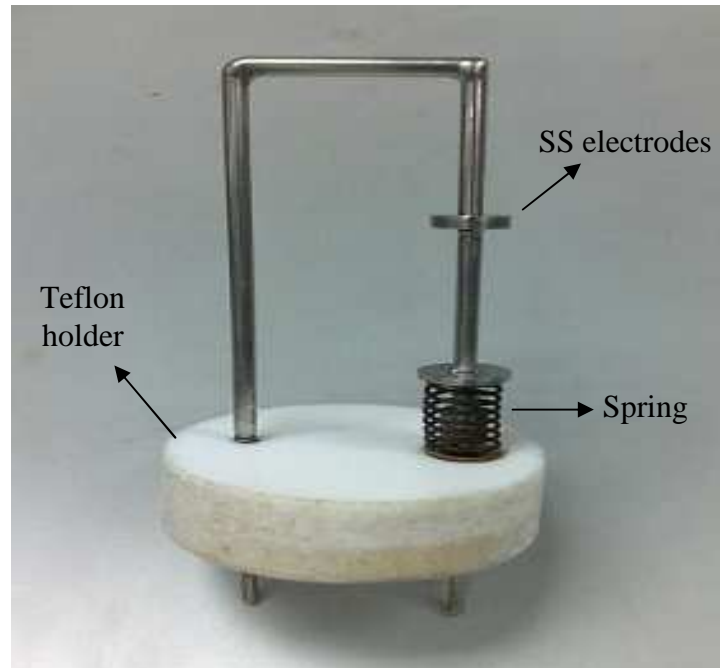
Figure 3.1 Conductivity and dielectric cell measurement.

The complex impedance plots (that is the plot of Z_i versus Z_r where Z_r and Z_i represent the real and imaginary parts of impedance respectively) were used for the determination of the bulk impedance of the samples as a function of temperature between 303 K and 423 K. The electrical conductivity was calculated using the relation,

$$\sigma_{dc} = \left(\frac{1}{R_b} \times \frac{t}{A} \right) \tag{3.1}$$

Here t is the thickness and A is the area of the film. R_b is the bulk resistance of the film derived from the intercept of the impedance plot on the real axis (see Fig 3.2). The equipment for measuring the impedance was the HIOKI LCZ Hi-Tester that operates from 50 Hz to 1 MHz.
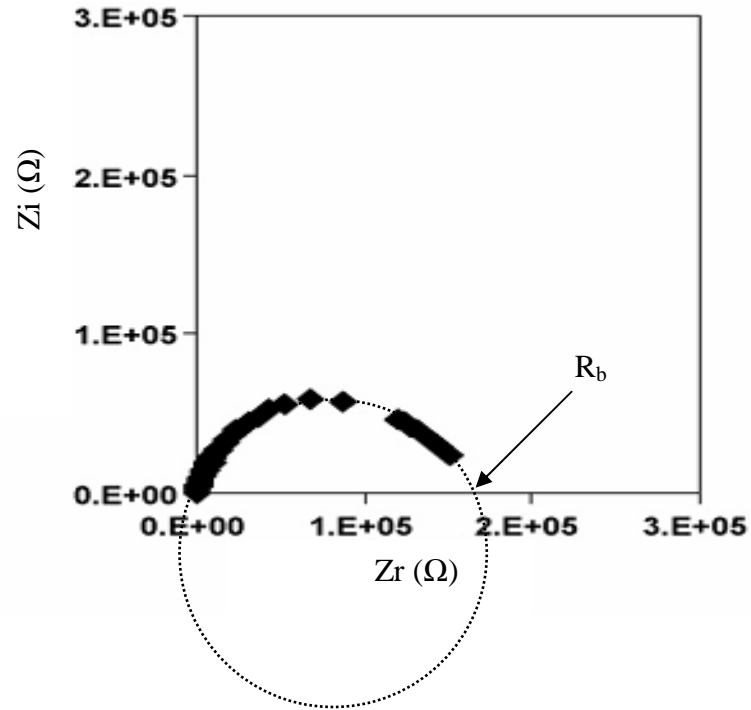
Figure 3.2 Cole-Cole plot for PVA:chitosan blend [Kadir et al., 2010].

The dielectric parameters such as dielectric constant (ε'), dielectric loss (ε''), loss tangent (tanδ), complex electric modulus (M' and M'') and AC conductivity was derived from the impedance-related functions as follows:

$$\varepsilon' = \frac{Z_i}{\omega C_\circ (Z_r^2 + Z_i^2)} \qquad (3.2)$$

$$\varepsilon'' = \frac{Z_r}{\omega C_\circ (Z_r^2 + Z_i^2)} \qquad (3.3)$$

$$Tan\delta = \frac{\varepsilon''}{\varepsilon'}$$

(3.4)

$$M' = \frac{\varepsilon'}{(\varepsilon'^2 + \varepsilon''^2)} = \omega C_o Z_i$$

(3.5)

$$M'' = \frac{\varepsilon''}{(\varepsilon'^2 + \varepsilon''^2)} = \omega C_o Z_r$$

(3.6)

$$\sigma_{ac} = \omega \varepsilon_\circ \varepsilon'' = \left[\frac{Z_r}{Z_r^2 + Z_i^2} \right] \times \left(\frac{t}{A} \right)$$

(3.7)

Here C_o is vacuum capacitance of the cell and is equal to $\varepsilon_o A / d$, where ε_o is permittivity of free space, A and d are the area and the thickness of the sample respectively and $\omega = 2\pi f$, where f is frequency.

3.4 X-ray diffraction (XRD) Analysis

X-ray technology has more than a hundred years of history and its discovery and development has revolutionized many areas of modern science and technology. The phenomenon of X-ray diffraction by crystals was discovered in 1912 by Max von Laue. The diffraction condition in a simple mathematical form, which is now known as the Bragg law, was formulated by Lawrence Bragg in the same year. X-rays are electromagnetic radiation with a wavelength in the range of 0.01–100 A°. The wavelength of typical X-rays used in X-ray diffraction is in the vicinity of 1 A°, which is comparable to the range of interatomic spacing in crystals. When a monochromatic X-ray beam hits a sample, in addition to absorption and other phenomena, it generates

scattered X-rays with the same wavelength as the incident beam. This type of scattering

is also known as elastic scattering or coherent scattering. Bragg law is a simple way to

describe the diffraction of X-rays by a crystal. In Figure 3.3, the incident X-rays hit the

crystal planes with an incident angle θ and reflection angle θ. The diffraction peak is

observed when the Bragg condition is satisfied:

$$n\lambda = 2\,d\,\sin\theta \qquad (3.8)$$

where λ is the X-ray wavelength, θ is the angle between the X-ray beam and the

atomic planes, and n represents the order of diffraction, a whole number.
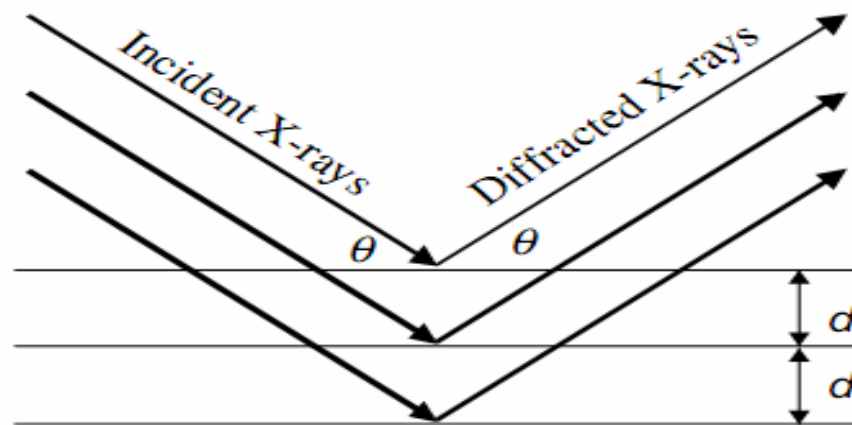
Figure 3.3 The incident X-rays and reflected X-rays make an angle of a symmetric to the normal of crystal plane (He, 2009).

 Most polymers are semicrystalline; that is a certain fraction of the material is

amorphous, while the remainder is crystalline. X-ray diffraction (XRD) analysis can

offer a wide range of information on crystal structure, crystal orientation, crystallinity,

crystallite size and phase changes of materials which are characterized by the presence

of sharp diffraction rings or peaks. In amorphous materials, there is no long-range order present; however, the non-crystalline samples are characterized by one or two broad "halos" [Rajendran et al., 2008]. In the present study, the X-ray diffraction method has been used to identify complex formation between the polymer and the salt as well as to study the effect of Al_2O_3 nano-sized particles on the crystallinity of nano-composite polymer electrolytes (NCPEs). XRD was carried out using a Siemens D5000 X-ray diffractometer with operating voltage and current of 40 kV and 40 mA respectively. The wavelength of the monochromatic, X-ray beam is 1.5406 A° and the glancing angles were in the range of $5° \leq 2\theta \leq 80°$ with a step size of 0.1°. The SPE and NCPE cast films were adhered onto glass slides for XRD measurement. Malathi et al. (2010) used XRD method to investigate the complexation between PVA and $LiCF_3SO_3$ as depicted in Fig 3.4. They explained the broadening and decrease of crystalline peak of PVA on the basis of complexation between PVA and $LiCF_3SO_3$ salt.
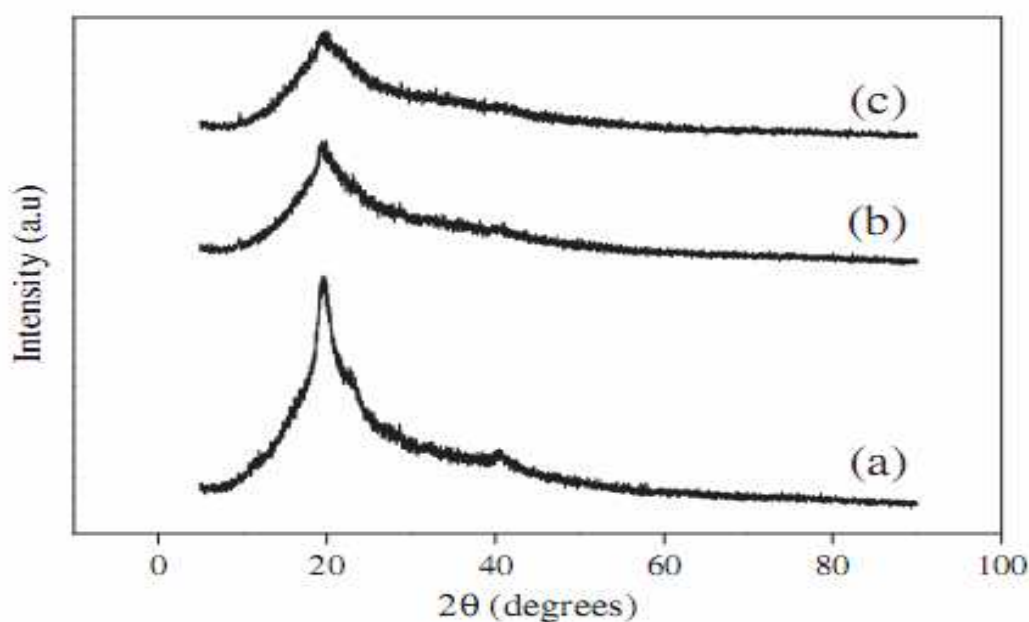
Figure 3.4 XRD pattern of PVA:LiCF$_3$SO$_3$ polymer electrolytes for (a) 95:05, (b) 85:15 and (c) 75:25 (Malathi et al., 2010).

3.5 Ultraviolet -visible absorption spectroscopy (UV-Vis)

Ultraviolet (UV) and visible radiation (380-780 nm) comprise only a small part of the electromagnetic spectrum, which includes such other forms of radiation as radio, infrared (IR), cosmic, and X rays. When radiation interacts with matter, a number of processes can occur, including reflection, scattering, absorbance, fluorescence/phosphorescence (absorption and reemission), and photochemical reaction (absorbance and bond breaking). In general, when measuring UV-visible spectra, we want only absorbance to occur. Because light is a form of energy, absorption of light by matter causes the energy content of the molecules (or atoms) to increase (Owen, 2000).

The unique optical properties of metal nanoparticles originate from the collective oscillations of conduction electrons, which, when excited by electromagnetic (EM) radiation, are termed surface plasmon resonances (SPR). The factors that collectively lead to these oscillations are: 1) acceleration of the conduction electrons by the electric field of incident radiation, 2) presence of restoring forces that result from the induced polarization in both the particle and surrounding medium, and 3) confinement of the electrons to dimensions smaller than the wavelength of light. The electric field of the incident EM radiation displaces the particle's electrons from equilibrium and, in turn, produces a restoring force that results in oscillatory motion of the electrons with a characteristic frequency, that is, the SPR frequency (Evanoff Jr and Chumanov , 2005).

UV–vis absorption spectra are known to be quite sensitive to the formation of silver nanoparticles. Investigation on the optical properties of silver nanoparticles has been done extensively in recent years, because the silver nanoparticles strongly absorb in the visible region due to surface plasmon resonance (SPR) (Kim et al., 2005). Gautam and Ram (2010) used UV-vis technique to investigate the formation of metallic silver nanoparticle in PVA medium as shown in Fig 3.5.
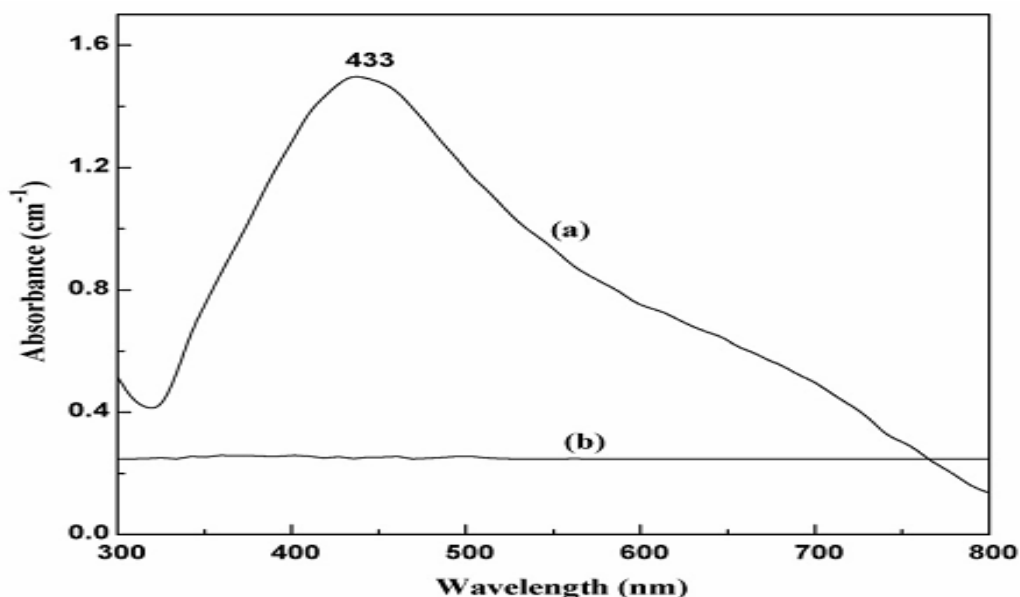
Figure 3.5. Optical absorbance in (a) Ag-PVA colloid solution and (b) pure PVA (Gautam and Ram, 2010).

The UV-vis spectra of solid polymer electrolytes (SPE) and nanocomposite solid polymer electrolyte (NCPEs) films containing silver triflate have been recorded using a Jasco V-570 UV-Vis-NIR spectrophotometer in the absorbance mode over the wavelength range from 190 to 900 nm.

3.6 Scanning Electron Microscopy (SEM) and Energy Dispersive Analysis of X-ray (EDX)

Electron Microscopy (EM) can be defined as a specialized field of science that employs the electron microscope as a tool and uses a beam of electrons to form an image of a specimen. Electron Microscopy (EM) is operated in vacuum and focuses the electron beam and magnifies images with the help of electromagnetic lenses. SEM is able to investigate surface structure and one of the advantages is that the range of magnification is wide allowing the investigator to easily focus on an area of interest of the sample

(Stadtländer, 2007). When an electron beam is focused on a specimen, the electrons are absorbed or scattered by the specimen, and secondary electrons, Auger electrons, characteristic X-rays and backscattered electrons are emitted from the sample during bombardment (Fig. 3.6) (Xu et al., 2007). In brief, the scanning electron microscope generates an image with the help of secondary electrons which can be detected by SEM (Stadtländer, 2007).

The application of scanning electron microscope combined with Energy Dispersive analysis of X-ray (SEM-EDX) is a powerful technique for the characterization of complex materials. On the loss of electron energy, X-ray fluorescence or Auger electron emission occur, which are very useful for element analysis. Both the secondary electrons and the Auger electrons have relatively low energy; arise from atoms close to the specimen surfaces. The release of X-rays creates spectral lines that are highly specific to individual elements; thus most of the chemical elements can be identified by EDX (Williams and Carter, 2009).
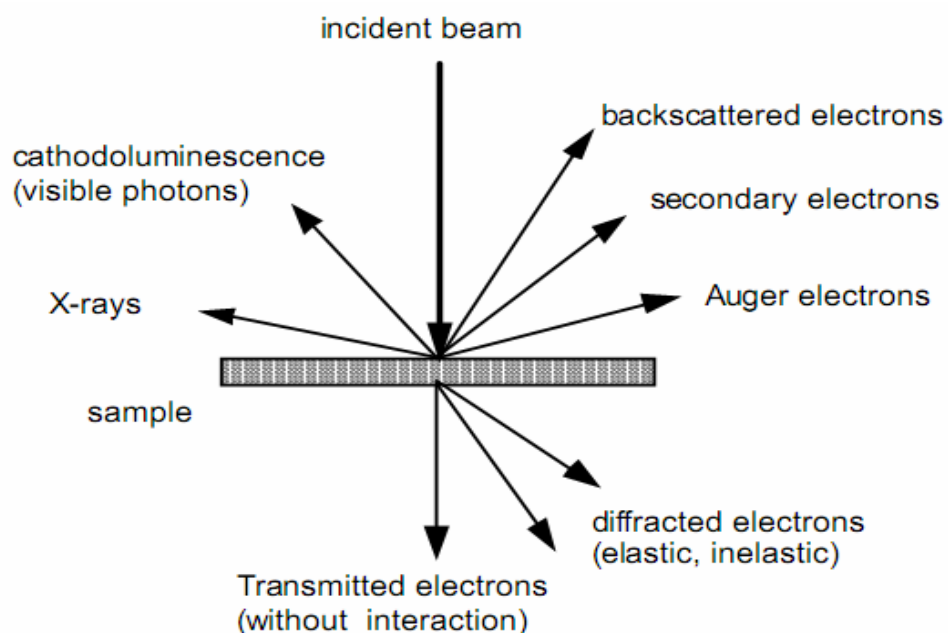
Figure 3.6 The interactions of an electron beam and sample atoms generating a variety of signals (Xu et al., 2007)**.**

The combined usage of SEM-EDX is an attempt to understand the structural and compositional complexity of the samples. The morphology and surface composition of SPEs and NCPEs were characterized by scanning electron microscopy (SEM) and energy dispersive analysis of X-rays (EDX) to combine structure-property relationship between electrical and structural properties. A scanning electron micrograph (SEM) was taken using Leica 440 scanning electron microscope to study morphological appearance. The microscope was fitted with energy dispersive analysis of X-rays (EDX), Oxford Instrument (LINK ISIS) to detect the overall chemical composition of solid chitosan electrolyte membrane. Before observation, the SPE and NCPE films were attached to aluminum holder using a conductive tape, and then coated with a thin layer of gold. Recently Wei et al., (2009) investigated silver nanoparticle leakages to the surface of the film in chitosan:AgNO₃, using SEM and EDX method as depicted in Figure 3.7(a-b).
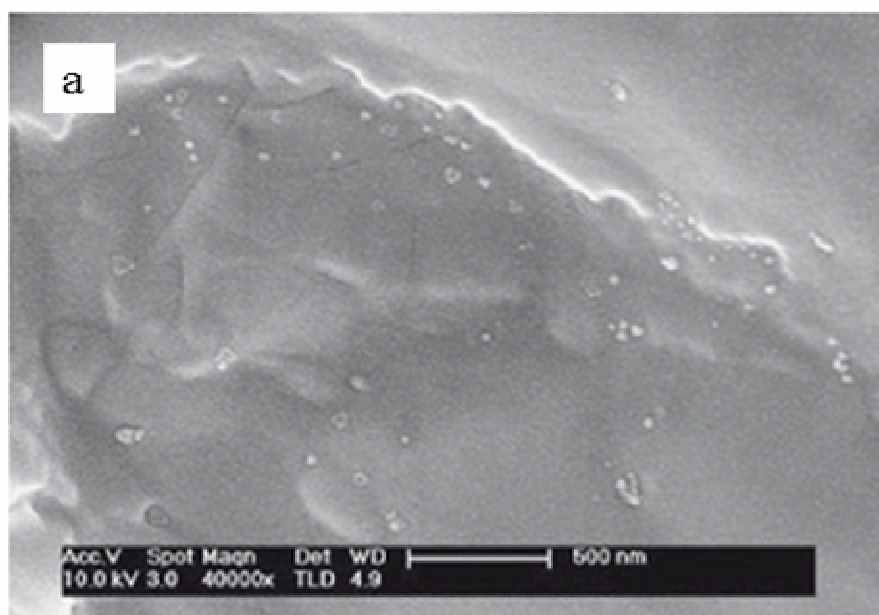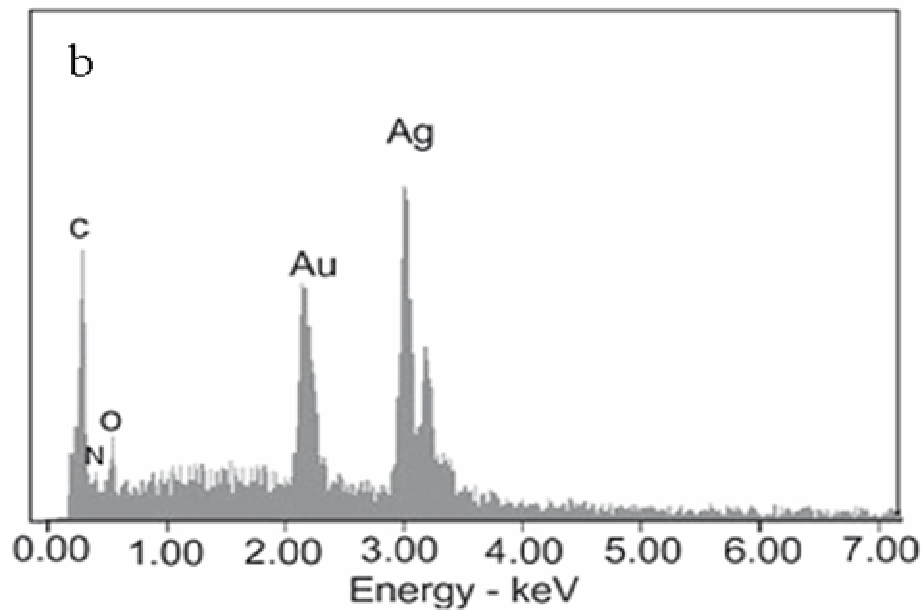
Figure 3.7 (a) SEM image and (b) EDX of the film of chitosan:AgNO₃ (Wei et al., 2009)**.**

3.7 Transmission Electron Microscopy (TEM):

Transmission electron microscopy (TEM) is considered the best available imaging technique for analysis of the internal structure, spatial distribution of the various phases, and views of the defect structure through direct visualization especially for thin films (Ray and Okamoto, 2003). In TEM operations, electrons interact strongly with atoms by elastic and inelastic scattering. The specimen must therefore be very thin, typically of the order of 5–100 nm for 100 keV electrons, depending on the density and elemental composition of the object and the resolution desired. Thus, TEM can provide high resolution because elastic scattering is an interaction process that is highly localized to the region occupied by the screened Coulomb potential of an atomic nucleus. Most of the inelastically scattered electrons normally pass through the objective diaphragm in the bright-field mode. Inelastically scattered electrons do not, however, contribute to high-resolution image details because the inelastic scattering is less localized. In the

elastic process the electrons interact with the electrostatic potential of nuclei of atoms. This potential deviate the trajectory of incident electrons without any appreciable energy loss; only the direction is changed. In fact a small loss occurs because of the change of the momentum. In this case all the electron beams can be collected to form an image of the specimen. However, in the inelastic case energy of the incident electron may be transferred to internal degrees of freedom in the atom or specimen in several ways. This transfer may cause excitation or ionization of the bound electrons, excitations of free electrons or lattice vibrations and possibly heating or radiation damage of the specimen (Reimer and Kohl, 2008).

Transmission electron microscopy (TEM) images of the polymer electrolyte containing silver salt were recorded using a LEO LIBRA (accelerating voltage 120 kV) instrument. A drop of the solution of chitosan-silver triflate electrolyte was placed on a carbon coated copper grid and dried at room temperature after removal of excess solution using a filter paper. Vimala et al., (2010), used TEM method to observe the silver nanoparticle formation and distribution in chitosan:$AgNO_3$ nanocomposite as depicted in Fig. 3.8.
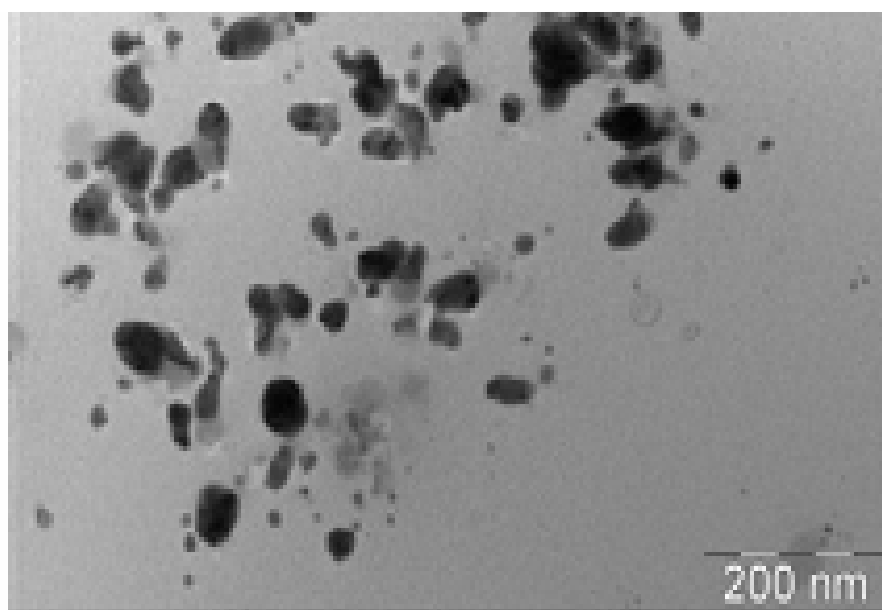
Figure 3.8 Transmission electron images of silver nanoparticles of chitosan-silver nanocomposite (Vimala et al., 2010).

3.8 Summary

In this chapter the preparation method of solid polymer electrolytes based on chitosan:XCF_3SO_3 (X = Ag^+, Na^+ and Li^+) and nanocomposite solid electrolytes ((1-x)(0.9CS:0.1AgTf)-xAl_2O_3 ($0.02 \leq x \leq 0.1$), (1-x)(0.9CS:0.1NaTf)-xAl_2O_3 ($0.02 \leq x \leq 0.1$) and (1-x)(0.9CS:0.1LiTf)-xAl_2O_3 ($0.02 \leq x \leq 0.1$)), have been clearly described. The benefit of XRD analysis is to investigate the effect of inorganic salts on chitosan crystalline structure, as well as to investigate the effect of Al_2O_3 nanoparticle on the crystallinity of SPEs. Scanning electron microscopy and energy dispersive analysis of X-rays (EDX) have been used to observe the surface morphology of SPEs and NCPEs. SEM is able to detect the phase separation in NCPEs. UV-vis spectrometry and transmission electron microscopy (TEM) are useful to detect the formation of silver nanoparticles in SPEs and NCPEs including silver triflate ($AgCF_3SO_3$) as the doping salt. Finally the electrical impedance spectroscopy (EIS) was used to study the electrical properties of all the SPE and NCPEs.